DOI: 10.1002/chem.200501071

A Counterintuitive Structural Effect of Metal–Metal Bond Protonation and Its Electronic Underpinnings

Andrew D. Phillips,[a] Andrea Ienco,[a] Joachim Reinhold,[b] Hans-Christian Böttcher,[c] and Carlo Mealli*[a]

In memory of Carlo Floriani

Abstract: Protonation across the metal–metal bond in the complexes $[(CO)_2M(\mu\text{-dppm})(\mu\text{-P}t\text{Bu}_2)(\mu\text{-H})\text{-}M(CO)_2]$ (M = Fe or Ru, dppm = $Ph_2PCH_2PPh_2$) induces M–M bond shortening of up to about 0.05 Å. DFT calculations on simplified iron models reproduce this trend well. Conversely, the computations show that the M–M distance in the dimer $[\{Cp^*Ir(CO)\}_2]$ lengthens with two consecutive protonations, but there are no crystal structure determinations to highlight the effects on the Ir–Ir bond. DFT calculations and the analogous cobalt system confirm that the transformation of a two-electron, two-center (2e–2c) bond into a 2e–3c bond is accompanied by the predicted elongation. An MO analysis indicated similar nature and evolution of the M–M bonding these cases. In particular, the HOMOs of the mono-hydrido cations $[Cp(CO)M(\mu\text{-H})M(CO)Cp]^+$ (M = Ir, Co) have evident M–M bent-bond character, and hence subsequent protonation invariably causes a decrease in the bond index. The Fe_2 and Co_2 systems have also been analyzed with the quantum theory of atoms in molecules (QTAIM) method, but in no case was an M–M bond critical point located unless an artificially shorter M–M distance was imposed. However, the trends for the atoms-in-molecules (AIM) bond delocalization indexes δ_{M-M} confirm the overall M–M bond weakening on protonation. In conclusion, all the computational results for the iron system indicate that the paradigm of a direct correlation between bond strength and distance is not always applicable. This is attributable to a very flat potential energy surface and various competing effects imposed by the bridging ligands.

Keywords: density functional calculations · hydrido ligands · iron · metal–metal interactions · protonation

Introduction

Transition-metal hydrides have received substantial attention over the past two decades for their role in formation, activation, and storage of hydrogen.[1] Particularly relevant to biology and catalysis are hydrogenation processes at dinuclear frameworks. In this context, we mention our recent DFT and NMR mechanistic study of the double reversible activation of H_2 over the Rh_2S_2 core.[2] At the biological level, the hydrogenases are comparably functional. In particular, the active site of Fe-only hydrogenases features a cooperative pair of iron centers, which in the early stage involve a bridging hydride intermediate.[3] Rauchfuss et al., in developing models of the latter, demonstrated that the Fe–Fe distance elongates by about 0.05 Å when the anion $[Fe_2(S_2C_3H_6)(CN)(CO)_4(PMe_3)]^-$ is protonated in the bridging region.[4]

Hydrido-bridged M–M bonds have received much theoretical attention, aimed to provide an adequate description of the electron redistribution at the three centers.[5] However, there are only a few structural reports on pairs of bimetallic precursors and hydrogenated derivatives, a selection of which is given in reference [6]. Elongation of the M–M dis-

[a] Dr. A. D. Phillips, Dr. A. Ienco, Dr. C. Mealli
Istituto di Chimica dei Composti Organo Metallici (ICCOM-CNR)
Via Madonna del Piano 10, 50019 Sesto Fiorentino (Firenze) (Italy)
Fax: (+39) 522-5203
E-mail: carlo.mealli@iccom.cnr.it

[b] Prof. J. Reinhold
Wilhelm-Ostwald-Institut für Physikalische und Theoretische Chemie
Universität Leipzig, 04103 Leipzig (Germany)

[c] Priv.-Doz. H.-C. Böttcher
Department Chemie und Biochemie
Ludwig-Maximilians-Universität München
81377 München (Germany)

Supporting information for this article is available on the WWW under http://www.chemeurj.org/ or from the author: Tabulated coordinates of all computationally optimized models. QTAIM diagrams of the models **1b**, **4b**, **12**,and **13**.

tance is generally predictable, since the two-electron, two-center (2e–2c) bond transforms into a 2e–3c one. In contrast, Puddephatt et al.[7] first pointed out the unexpected shortening of an Rh–Co bond on protonation (from 2.6858(2) to 2.6480(8) Å). The structures of parent dimer $[(CO)Rh(\mu\text{-}CO)(\mu\text{-}dppm)_2Co(CO)]$ (dppm = $Ph_2PCH_2PPh_2$) and its protonated derivative are shown in Figure 1 (data

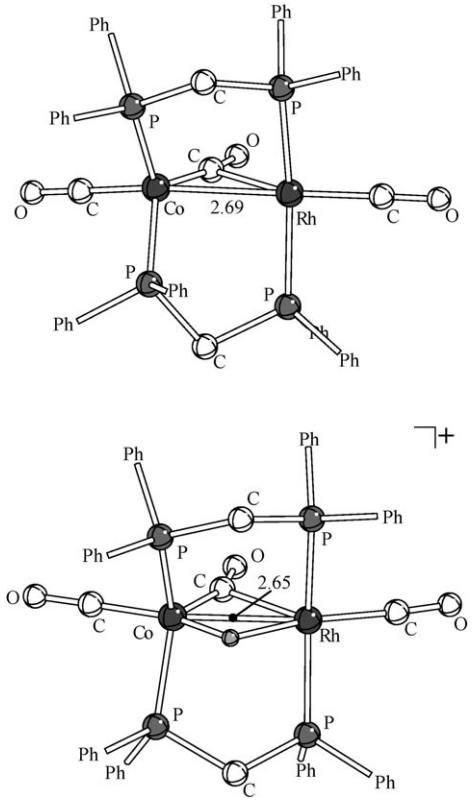

Figure 1. Structures of parent dimer $[(CO)Rh(\mu\text{-}CO)(\mu\text{-}dppm)_2Co(CO)]$ (dppm = $Ph_2PCH_2PPh_2$) and its protonated derivative.

obtained from the Cambridge Structural Database[8]). Theoretical analysis of this heterodinuclear system, which approximately combines a T-shaped RhL_3) and a trigonal-pyramidal CoL_4 fragment, is complicated by the semibridging CO ligand and lack of symmetry.

One covalent or dative M–M σ bond must be present in the unprotonated precursor (possibly, a d^9–d^9 or d^8–d^{10} combination of metal configurations). Following protonation, the metal σ hybrids reorient somewhat toward the H bridge and form a 2e–3c bond, as indicated by the bending of the Co-Rh-$(CO)_{term}$ group and the more symmetrically bridging CO. For the precursor, the Rh=Co bond suggested by the total electron count of 32 is inconsistent with the orientation of the fragments which does not allow d_π–p_π overlap between Co and the planar-coordinated Rh centers. It was originally suggested[7] that protonation could activate a dormant M=M bond, but this remained unsupported by a subsequent theoretical analysis.[9] According to the latter, even the presence of a M–M σ bond in the precursor can be seriously questioned owing to the lack of a suitable HOMO[10] and the absence of the corresponding bond critical point (bcp; AIM analysis[11]). Thus, the shortening of the distance in the protonated derivative would simply stem from a newly formed 2e–3c interaction.[9] In the dirhodium analogue, the Rh–Rh distance is unaffected by protonation (2.739(1) versus 2.731(2) Å).[12] In this case, a quantum theory of atoms in molecules (QTAIM) analysis of the precursor showed that, on rearranging the CO bridge from symmetric to semibridging, the Rh–Rh bcp disappears.[13] In conclusion, an irrefutable explanation of the effects of M–M bond protonation is not available yet. In particular, the QTAIM approach seems to have evident difficulties in clarifying the nature of M–M bonding, especially in the presence of CO ligands, which subtract a significant amount of electron density away from the intermetallic region.[14]

The structures of the complexes $[(CO)_2M(\mu\text{-}dppm)(\mu\text{-}P\mathit{t}Bu_2)(\mu\text{-}H)M(CO)_2]$ (M = Fe (**1**),[15] Ru (**2**)[16]) and $[(CO)_3M(\mu\text{-}P\mathit{t}Bu_2)(\mu\text{-}CO)M(CO)_3]^-$ (M = Fe (**3**)[17]) together with those of their H-bridged derivatives (**4**–**6**, in that order),[17,18] provide new examples of M–M bond shortening on protonation. The extent of the effect (almost 0.05 Å in most cases) and the relatively symmetric metal environments encouraged us to perform specific DFT and AIM analyses to evaluate the electronic underpinnings of the phenomenon, especially by focusing on the diiron species **1** and **4**. By idealizing the H bridges as protons and the phosphido anion as a four-electron donor, the dimers consist of two

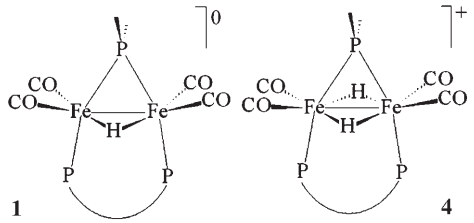

connected L_4M d^8 fragments, isolobal with CH_2.[19] Thus, an Fe=Fe bond could exist in the hypothetical monoanionic precursor $[(CO)_2Fe(\mu\text{-}dppm)(\mu\text{-}P\mathit{t}Bu_2)Fe(CO)_2]^-$ (**7**) with σ and π components analogous to those of the C=C bond in ethylene.

Figure 2 illustrates the above-mentioned isolobal analogies, which are eventually extended to pairs of $Cp(L)M$ d^8 fragments, because the known complex $[\{Cp^*Ir(CO)\}_2]$ (**8**) has been reported to accept two protons across the Ir–Ir linkage in two separate steps.[20]

Of the iridium series **8**–**10**, only the precursor has been structurally characterized. In fact, this species features two

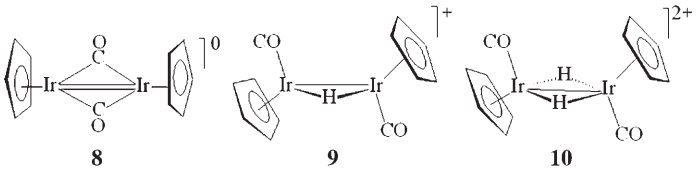

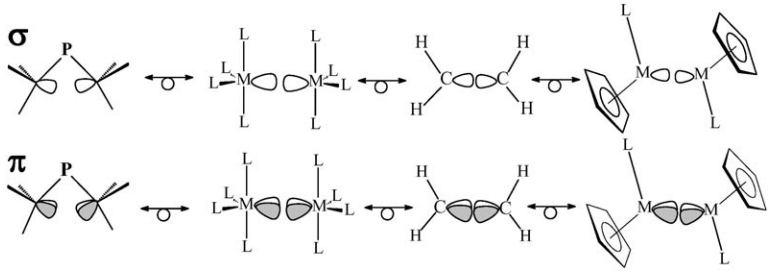

Figure 2. Isolobal relationships between L_4M d^8, methylene, and Cp(L)M d^8 fragments.

bridging CO ligands, but spectroscopic evidence suggests that these are shifted to terminal positions on protonation.[20] It therefore seems challenging to compare with computational methods the behavior of the diiron and diiridium systems with respect to the effects on the intermetallic distance.

The analysis is then extended to the analogous dicobalt system (models **11**–**13**), for which no protonation chemistry is reported, while there are several structural reports of the precursor **11** with various substituents on the Cp rings.[21] In our view, the contiguity of the metals Fe and Co makes the study of the latter system even more appropriate than that for the iridium system.

We present systematic DFT calculations for the abovementioned dinuclear Fe, Ir, and Co complexes and interpret the M–M interactions in terms of perturbation theory and by chemical intuition. Additionally, a QTAIM approach[11] was adopted, also because the method has been scarcely applied to 3e–3c bonds formed by two metals and one bridging hydride. An example is the anion $[(CO)_5Cr(\mu\text{-}H)Cr(CO)_5]^-$, in which the long Cr–Cr distance (ca. 3.3 Å) is at the limit of bonding/nonbonding interactions,[22] and the other relatable study is that on $[CpMnHSiCl_3]$, in which the MnHSi ring contains only one metal center.[23]

Results and Discussion

Iron dimers: mono- and diprotonated species: The first calculations were carried out for models based on the experimental structures of **1** and **4**[15,18] with H atoms replacing all the bulky substituents on phosphorus. Figure 3 shows optimized models **1a** and **4a**. The geometries compare satisfactorily; in particular, the trend towards a shorter Fe–Fe distance is respected in the doubly H bridged species ($\Delta r = 0.02$ versus 0.05 Å, in the computed and experimental structures, respectively).

Consistent results were also obtained for the further simplified models **1b** and **4b** (Figure 4), in which two PH_3 ligands replace the bridging dppm. This result excludes that the origin of this effect is due to the small and constrained bite angle of the dppm ligand.

The consistency of the simpler and more symmetrical models facilitates the examination of other subtle effects on the geometry. For example, **4b** has almost C_{2v} symmetry, while in **1b** (quasi-C_s) the Fe_2P_{bridge} plane is no longer a mirror plane, not only because of the presence of only one H bridge. In fact, the two $Fe(PH_3)(CO)_2$ fragments are rotated by about $\tau = 8°$ around their inner Fe–P vectors, so that the two L_4M σ hybrids are reoriented toward

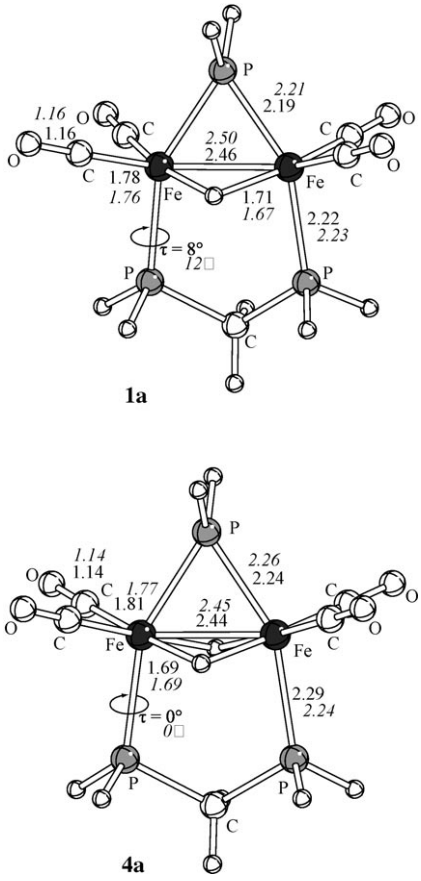

Figure 3. Optimized models **1a** and **4a** with computed and average experimental (italic) parameters.

the single H bridge and favor, in principle, a stronger 2e–3c bond (σ–π rehybridization also occurs, vide infra). Another noticeable trend is the elongation of all the M–L bonds on going from **1b** to **4b**. In fact, the distances $Fe-P_{br}$, $Fe-P_{term}$, and Fe–CO increase (on average) from 2.19 to 2.23 Å, 2.23 to 2.30 Å, and 1.78 to 1.81 Å, respectively. Correspondingly, the C–O distances shorten by about 0.02 Å, as reflected in the larger CO wavenumbers (by about 100 cm^{-1}) of the bis-H derivative. In conclusion, the added proton seems to subtract electron density from the metal centers and hence reduces backdonation to both the terminal CO and phosphine ligands.

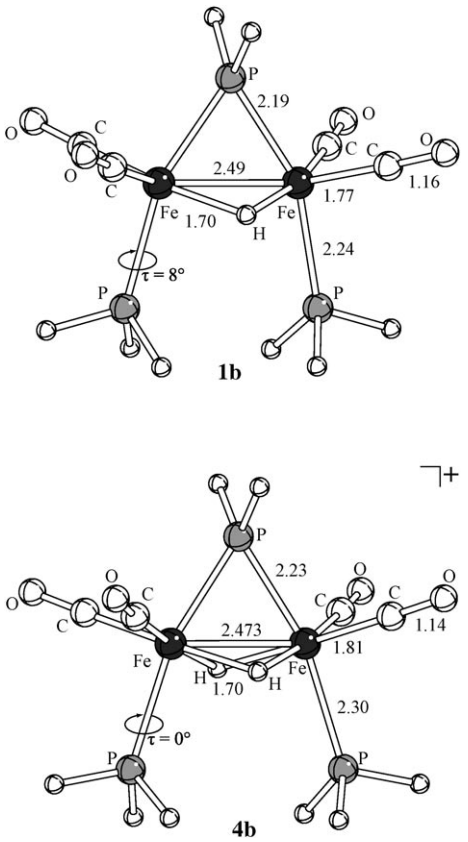

Figure 4. Optimized models **1b** and **4b** with computed parameters.

With the goal of determining the geometric parameters which directly affect the M–M distance, models **1b** and **4b** were optimized again by imposing a fixed Fe–Fe distance significantly longer (2.65 Å) or shorter (2.33 Å) than that at equilibrium. In the latter case, no convergence was obtained for the bis-H species. In general, the bridging Fe–H and Fe–P distances undergo modest changes, since the necessary structural rearrangements occur at the Fe-bridge-Fe angles. For the mono-H derivative, however, there is an evident effect on the τ rotation of each $Fe(PH_3)(CO)_2$ fragment (see Figure 4). This is practically zero at the long separation, but it is maximized (ca. 12°) at 2.33 Å. The total energy variations are rather small in any case. For the bis-H derivative **4b**, the elongation of the Fe–Fe distance to 2.65 Å causes an energy increase of 2.7 kcal mol^{-1}. For the mono-H species **1b**, the ΔE values are 2.4 and 1.4 kcal mol^{-1} at 2.33 and 2.65 Å, respectively. Moreover, in the more restricted range of distances 2.42–2.57 Å, the variation of the potential energy surface (PES) is no more than 0.5 kcal mol^{-1}, and this suggests a quite flexible intermetallic framework for both the singly and doubly H-bridged species.

The Mayer bond index[24] of the Fe–Fe bond is significantly greater for **1b** than for **4b** (0.98 versus 0.75). Also, the Fe–Fe reduced overlap populations from simple EHMO calculations[25,26] follow the trend (0.27 versus 0.11, for **1b** and **4b**, respectively) and indicate that bond length and strength are not directly correlated. A similar conclusion was reached by us in a previous theoretical analysis for the classical $[M_3(CO)_{12}]$ systems (M = Fe, Ru, Os).[27] In the trinuclear iron cluster, the unique CO-bridged Fe–Fe bond is shorter than the unbridged ones in spite of the reversed bond indexes.

Structure of the unprotonated precursor $[(CO)_2Fe(\mu\text{-}Ph_2PCH_2PPh_2)(\mu\text{-}PtBu_2)Fe(CO)_2]^-$: The d^8–d^8 anionic species of the type $[(CO)_2Fe(\mu\text{-dppm})(\mu\text{-}PtBu_2)Fe(CO)_2]^-$ (**7**) can be considered as an inorganic analogue of ethylene (Figure 2). A similar point was raised by Hoffmann, who hypothesized for $Fe_2(CO)_8$ the unbridged structure **I** with a Fe=Fe bond. As an alternative, the structure **II** with two CO bridges was also considered.[19] Later computations showed that various other conformers are also possible.[28–30]

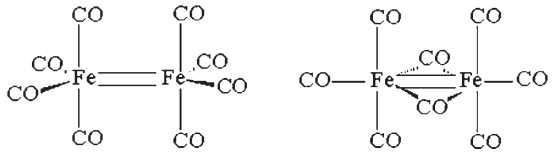

I II

In the absence of structural information on the hypothetical precursor of **1** and **4**, two isomers were optimized at the DFT level of theory with one (**7a**) or two CO bridges (**7b**; Figure 5). Models with discrete PH_3 ligands in place of dppm have consistent geometries.

Complex **7a** has a semibridging CO ligand (Fe1-C1-O1 151°), similar to that of the complex in Figure 1[7] and the dirhodium analogue.[12] On the other hand, the doubly bridged isomer **7b** is energetically disfavored with respect to **7a** by about 18 kcal mol^{-1}, and does not even correspond to a minimum, in view of two imaginary frequencies. However, the significantly shorter Fe–Fe distance in **7b** ($\Delta d = 0.12$ Å) suggests multiple-bond character which is not present in **7a**, in which the potential Fe=Fe double bond remains hidden. In other words, the structure of the most stable unprotonated precursor is inappropriate for simultaneous σ and π bonding (see Figure 2). Some associated electronic problems are addressed in the qualitative MO analysis (vide infra).

There is a strong correlation between the computed CO stretching vibrations and the Fe–CO bond lengths in the series of model compounds. As expected, the semibridging or bridging CO ligands have the lowest frequencies, while those of the terminal CO ligands progressively increase in going from the unprotonated to the mono- and diprotonated derivatives. The decreased electron density on the metal center is consistent with the d^8, d^7, and d^6 configurations attributable to the Fe centers in **7**, **1**, and **4**, respectively. This is indirectly confirmed also by the protonation energies, which were roughly estimated by excluding the effects of the solvent and in the absence of a corresponding base. As is predictable from the increasing oxidation number, the addition of the first proton is significantly more exothermic than that of the second proton (−342.4 and −245.5 kcal mol^{-1} for **7a**→**1a** and **1a**→**4a**, respectively).

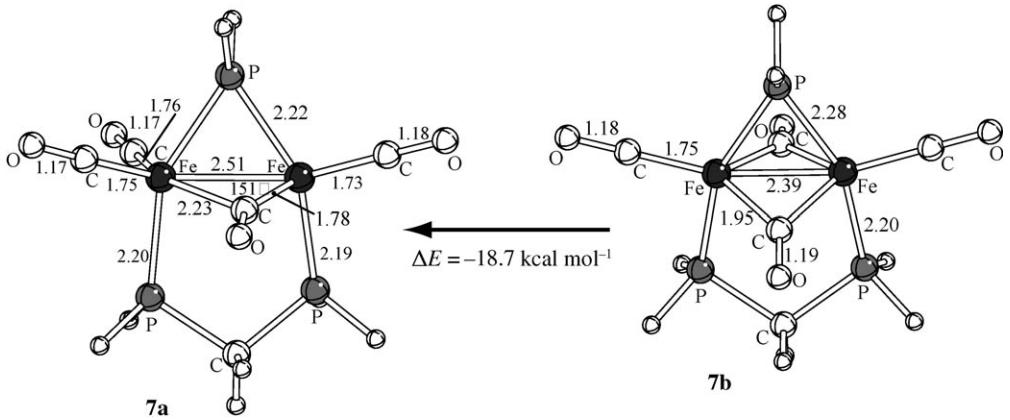

Figure 5. DFT optimized isomers **7a** and **7b**.

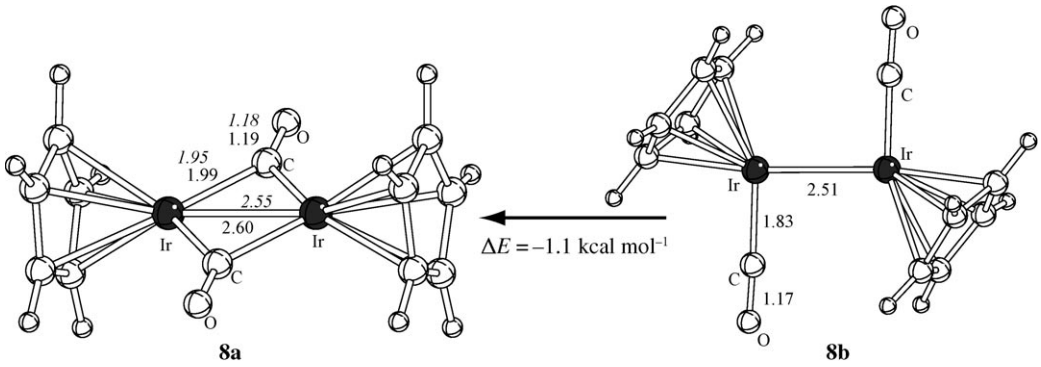

Figure 6. DFT optimized isomers **8a** and **8b**.

Protonation of Group 9 dimers [{CpM(CO)}$_2$] and isolobal main-group analogues: Stepwise protonation of [{Cp*Ir(CO)}$_2$] (**8**) yields **9** and **10**.[20] The precursor has a doubly CO bridged structure similar to those of several Co-based analogues with variously substituted Cp ligands.[21] DFT calculations were carried out on the precursors and the protonated derivatives (never structurally characterized) of both metals to verify the effects on the M–M distance. Unsubstituted Cp ligands were invariably used.

As for the iron precursor **7**, two iridium isomers were optimized as real minima. The CO-bridged model **8a** is slightly more stable (by 1.1 kcal mol^{-1}) than the one with terminal CO groups (**8b**) as shown in Figure 6. Remarkably, a significantly longer Ir–Ir distance in **8a** (2.60 versus 2.51 Å) suggests that an actual M=M bond can be realized in the absence of ligand bridges.

The calculations on the analogous Co-based precursor afforded only the bridged structure **11** (not shown), in which the Co–Co distance is somewhat longer than the experimental value[21a] (2.360 versus 2.322 Å). Other X-ray structures show that the separation increases with greater bulkiness of the Cp substituents.[21] This suggests that steric repulsion between opposite Cp and CO ligands plays an important role and that the unbridged dicobalt isomer may be considerably destabilized if the Co–Co distance is as short as that of a double bond.

The mono- and bis-H derivatives of diiridium (**9** and **10**, Figure 7) and dicobalt (**12** and **13**, not shown) were all optimized as real minima. In the former case, starting from the unbridged precursor **8b**, the Ir–Ir distance progressively increases from 2.51 Å to 2.59 (in **9**) to 2.72 Å (in **10**). This is consistent with two consecutive transformations of a 2e–2c into a 2e–3c M–M bond.

Since the unprotonated cobalt precursor **11** shows only the CO-bridged structure, only the final step of protonation is comparable to that of the iridium system. In any case, the elongation trend is fully confirmed (from 2.32 to 2.43 Å). In both cases, the Mayer bond indexes[24] (0.98 and 0.81 for **9** and **10** and 0.342 and 0.258 for **12** and **13**, respectively) suggest a direct correlation between M–M distance and bond strength, which does not apply to the diiron system. Another similarity between the Ir and Co systems concerns the progressively longer M–C and shorter C–O distances. Thus, metal backdonation to CO diminishes whenever the added proton transforms into a hydride.[31] The trend is well reflected by the CO stretching frequencies.[32]

The M–M distance computed for the protonated derivative [Cp(CO)Co(μ-H)Co(CO)Cp]$^+$ (**12**) is about 0.17 Å shorter than that in [(PH$_3$)(CO)$_2$Fe(μ-PH$_2$)(μ-H)Fe(CO)$_2$(PH$_3$)] (**1b**) in spite of the almost equal metal radii (Δ = 0.01 Å). The more contracted intermetallic region in the cobalt species is also reflected by the shorter Co–H$_{br}$ distan-

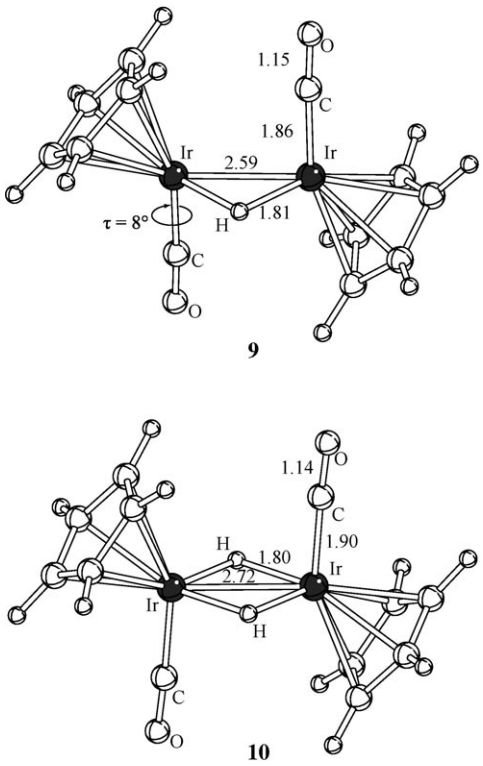

Figure 7. Optimized structures of **9** and **10** with computed parameters.

ces with respect to the Fe–H_{br} ones (1.64 versus 1.70 Å). On the other hand, these data are apparently in contrast with first and second protonation energies of the cobalt species (−220.4 and −131.5 kcal mol^{-1}, respectively) which are about 100 kcal mol^{-1} less exothermic than those of the corresponding iron species. Certainly, the presence of several P donors in the latter case is responsible for electron richer metal centers. Other influencing factors are the requirements of the bridging phosphido group, which is addressed below in the MO analysis.

The terminal Cp(CO)M fragments in both the monoprotonated Ir and Co species **9** and **11** are rotated by a few degrees with respect to the M–M axis, that is, the equivalent of the τ rotation in models **1a** and **1b**. As pointed out for the latter, this type of deformation strongly favors better overlap between the metal σ hybrids and the H 1s orbital and thus results in a more effective (stronger) 2e-3c bond. In this respect, constrained optimizations of the mono-H cobalt complex **12** were also carried out at different Co–Co distances, which were either shorter (2.24 Å) or longer (2.50 Å) than the equilibrium distance (2.36 Å). Again, a correlation is observed between the intermetallic distance and the somewhat different orientation of the terminal fragments (τ rotation). Moreover, a very flat PES is observed, as indicated by the ΔE values of +0.6 and +1.4 kcal mol^{-1} at the shortest and longest Co–Co separations, respectively.

Finally, in view of the analogy between d^8 ML_4 and CR_2 fragments (see Figure 2), the bonding in the present metal dimers is comparable to that in olefins.[19] Accordingly, the single and double protonation of the C=C bond of ethylene was computationally tested by systematically optimizing the species $C_2H_4/C_2H_5^+/C_2H_6^{2+}$, all of which were found to be minima. The progressive elongation of the C–C distance from 1.33 to 1.38 to 1.54 Å confirms that transformation of a 2e–2c into a 2e–3c bond weakens the interaction between the backbone atoms.

Qualitative MO analysis: Since the counterintuitive response to protonation on the diiron system is well reproduced by the DFT calculations, a detailed orbital analysis may highlight the electronic origin of the phenomenon, especially in comparison with the normal behavior of the Co and Ir systems. Figure 8 illustrates how one or two lateral

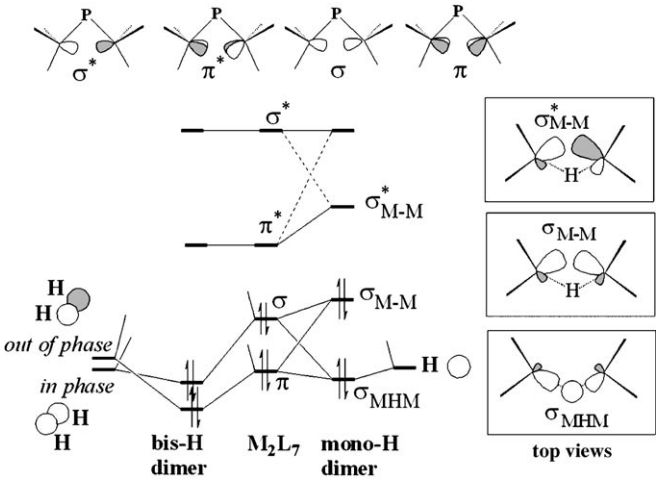

Figure 8. Comparative diagrams for the interaction of the frontier orbitals of a M_2L_7 fragment (middle) with one (right) or two (left) bridging H atoms.

hydrogen atoms perturb the central frontier MOs of a symmetric $L_3M(\mu\text{-}PH_2)ML_3$ moiety.

For two d^8-configured metal atoms, the in-phase combinations of d_π and σ hybrids are both populated, but the stabilization of a M=M bond requires a sufficiently large HOMO–LUMO gap. This is not warranted by the intrinsic high energy of the combining σ hybrids, which prevents the σ_{M-M} bonding combination from lying much lower than the d_π–d_π antibonding one (π* LUMO). Thus, a second-order Jahn–Teller distortion may be activated, as confirmed by the highly asymmetric structure of the diiron precursor **7a** (Figure 5), in which the M=M bond may actually be dormant. One lateral H bridge added to the ideal-C_{2v} precursor breaks one of the mirror symmetries and forces the mixing of the σ and π M–M bonding MOs (right side of Figure 8). Rehybridization is further enhanced by the significant τ rotation of the ML_3 fragments (as defined in Figures 3 and 4) and the overall 2e–3c bond is strengthened (see the lower box of Figure 8). Opposite to the H bridge, a bent σ_{M-M} bond (definitely nondormant) results from σ–π rehybridization (upper box), which is fully confirmed by the picture of

the HOMO obtained from the DFT coefficients (Figure 9a). The HOMOs of mono-H diiridium and dicobalt complexes **9** and **12** (Figure 9b) have a similar nature.

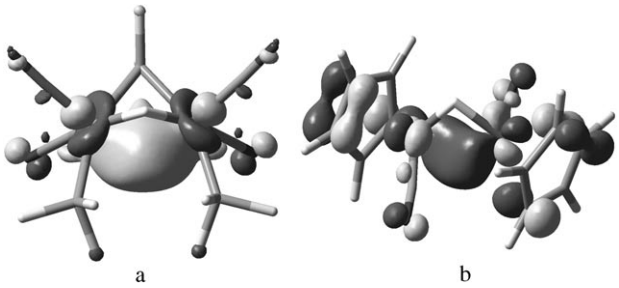

Figure 9. a) HOMO of the model $[(PH_3)(CO)_2Fe(\mu\text{-}PH_2)(\mu\text{-}H)Fe(CO)_2(PH_3)]$ (**1b**). b) HOMO of the model $[Cp(CO)Co(\mu\text{-}H)Co(CO)Cp]^+$ (**12**).

Interestingly, a similar π*/σ* mixing determines the final shape of the LUMO with a specific antibonding character for the bent M–M bond, as shown in the upper box of Figure 8. This level is occupied in the complex $[(CO)_2Co(\mu\text{-}dppm)(\mu\text{-}PPh_2)(\mu\text{-}H)Co(CO)_2]$[33] (**15**), which can be considered the analogue of two-electron-reduced diiron complex **1**. The M–M experimental distance in **15** (2.637(1) Å) is elongated by about 0.20 Å with respect to that in **1**. As expected for electron-rich systems, the DFT computed Co–Co distance is overestimated (by about 0.10 Å) for the model **15a**, which contains an H-substituted dppm ligand. In spite of the electron richer metal atoms, no protonation chemistry is reported for **15**. Provided that H^+ addition is possible, it is unlikely that H bridges are formed due to the absence of a bent M–M bond.

The various attractive and repulsive interactions activated by the occupied MOs could also be qualitatively monitored by tools such as interaction and Walsh diagrams, the MOOP table (overlap population orbital by orbital), and so on.[26b] For instance, the τ rotation enhances both the $\sigma_{M\text{-}H\text{-}M}$ and σ_{M-M} interactions (two-thirds of the M–M bonding is associated with the HOMO) and reduces the repulsion between pairs of $d_{x^2-y^2}$ orbitals belonging to the t_{2g} set. As shown in Figure 10, the antibonding combination becomes less destabilized with increasing τ, and this also justifies why the parameter is maximized at the shorter Fe–Fe distance of 2.33 Å and zero at 2.64 Å. However, other occupied MOs follow the opposite trend, so that the overall PES appears rather flat and featureless.

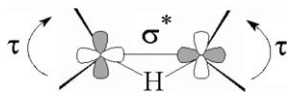

Figure 10. Orbital underpinnings of the stabilizing trend due to τ rotation.

As was already pointed out, the M–M distance appears definitely longer in the diiron than in the comparable Cp_2Co_2 complexes in spite of the almost equal radii. This is due to the different assembly of the two opposed ML_4 fragments, as exemplified in Figure 11, which compares a system with all terminal ligands (also applicable to a CpM derivative) with the phosphido-bridged analogue.

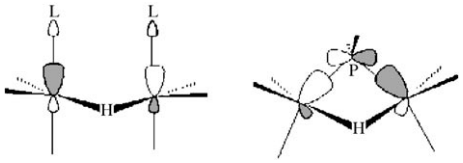

Figure 11. Comparison of selected orbital interactions with all terminal ligands with one phosphido bridge.

On the left side, the parallel and accepting metal hybrids are out of phase with respect to each other, that is, the combination is π* in character. Conversely, the interaction with the p_π orbital of the phosphido bridge (right side of Figure 11) imposes a significant reorientation of the metal hybrids toward each other, with some $\sigma\text{–}d_\pi$ mixing. As a consequence, the accepting combination acquires significant M–M σ* repulsive character, which is activated by the electron density donated by the phosphido bridge. The corresponding elongation of the intermetallic distance seems also to imply that the further elongating effect of protonation on an already stretched Fe–Fe bond can be much less evident.

We now briefly address the relation of the iron complexes discussed above with some of their formal derivatives in which a third, non-H bridge (CO, CH_2, or SO) substitutes for the second H bridge in **4**. The experimentally characterized compounds are $[(CO)_2Fe(\mu\text{-}Ph_2PCH_2PPh_2)(\mu\text{-}PCy_2)(\mu\text{-}H)(\mu\text{-}CO)Fe(CO)_2]$,[34] (**16**), $[(CO)_2Fe(\mu\text{-}Ph_2PCH_2PPh_2)(\mu\text{-}PtBu_2)(\mu\text{-}H)(\mu\text{-}CH_2)Fe(CO)_2]$,[16] (**17**), and $[(CO)_2Fe(\mu\text{-}Ph_2PCH_2PPh_2)(\mu\text{-}PtBu_2)(\mu\text{-}H)(\mu\text{-}SO)Fe(CO)_2]$[35] (**18**). At variance with the hydride bridge, all the new μ-type ligands have both σ-donor and π-acceptor capabilities, the latter being characterized by an empty p_π orbital (CH_2) or a π* level (CO and SO; for the latter the orthogonal π* level is occupied). Recall that the addition of a proton to **1** causes transfer of the Fe–Fe bonding electrons (see Figure 9a) to the resulting hydrido bridge (oxidative addition). In contrast, the new bridge in **16**–**18** carries a σ lone pair, which is strongly repulsive with the Fe–Fe bent bond. As shown in Figure 12, the problem is avoided if one of the two electron

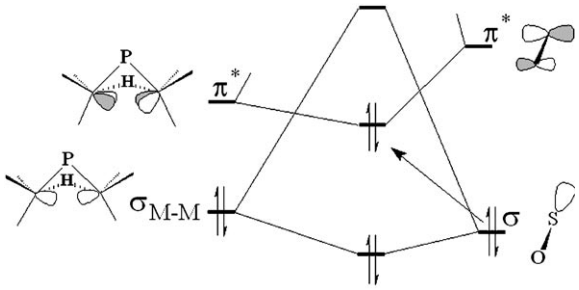

Figure 12. Interactions between the frontier MOs of the mono-H model **1b** and the σ-donor and the π-acceptor orbitals at the bridge.

pairs transfers into the π-bonding combination between the bridge p_π acceptor orbital (e.g., CO π*) and the metal-centered π* combination (ex-LUMO in Figure 8). Importantly, the partial population of the ex-LUMO level explains why in all three species **16**–**18**, the Fe–Fe distance (2.579(2), 2.496(1) and 2.613(1) Å, respectively) is about 0.1 Å longer than in the complexes **1** and **4**.

QTAIM analysis: The noncanonical behavior of the Fe_2 system on protonation was studied by using the quantum theory of atoms in molecules (QTAIM),[11] also with the aim of characterizing the electron-density topology in the region of the M–M bond. The detailed results will be reported elsewhere,[36] but we summarize here the relevant comparison of the Fe_2 and Co_2 systems because of the contiguity of the metals in the periodic table. The Ir_2 analogues could not be studied due to the lack of an appropriate basis set.

The connection between any two bonded atoms in the QTAIM method is signified by the appearance of a saddle point of minimum electron density ρ along the interatomic vectors, that is, a bond critical point (bcp).[11] For the mono- and bis-H diiron models **1b** and **4b**, (Figure 4), as well as the dicobalt models **12** and **13** (see the Ir_2 analogues in Figure 7), all the expected metal–ligand and intraligand bcp were located, and the corresponding ρ values correlate well with the bond lengths (see Supporting Information). In particular, the metal–ligand interactions appear to decrease from the mono- to the bis-H derivatives. These results are consistent with the trends for the optimized geometric parameters, which were already interpreted in terms of reduced π backdonation from the metals. The M–H interactions are almost unaffected by the second protonation, as shown by the corresponding bcp. Interestingly, the Co–H bcp in both **12** and **13** are characterized by electron densities which are somewhat higher than that of the corresponding Fe–H bcp, and thus follow the difference in bond lengths (1.63 versus 1.70 Å, respectively).

In none of the cases could an M–M bcp be located, similar to other complexes with chemically predictable M–M bonds.[14] Recall, in this respect, that no Rh–Co bcp could be detected[9] for the system [(CO)Rh(μ-CO)(μ-dppm)$_2$Co(CO)] (Figure 1),[7] which behaves identically to the diiron species on protonation. Other classical failures are $[Co_2(CO)_8]$[37] and $[Fe_2(CO)_9]$,[38] for which symmetry and perturbation theory arguments, as well as a detailed ab initio analysis,[39] support the presence of an, albeit weak, Fe–Fe bond. Conversely, the bcp has been detected for some dimetal carbonyl compounds (e.g., $[Mn_2(CO)_{10}]$) by using either theoretical[40] or experimental[41] determinations of the electron density. In particular, an experimental study on the complex $[Co_2(CO)_6(\mu\text{-}CO)(\mu\text{-}C_4O_2H_2)]$ revealed the Co–Co bcp, although the surface in the intermetallic region is quite flat.[42]

Interestingly, our AIM analysis shows incipient detection of the M–M bcp as a function of the M–M distance. Recall that for both the diiron and dicobalt systems, models with imposed short M–M distances were optimized with the goal of finding some correlation with other geometrical parameters (e.g., the τ rotation defined in Figures 3 and 4). The electron density profiles along the M–M vector of the mono-H complexes **1b** and **12** are depicted at the top and bottom of Figure 13, respectively. The black and gray lines

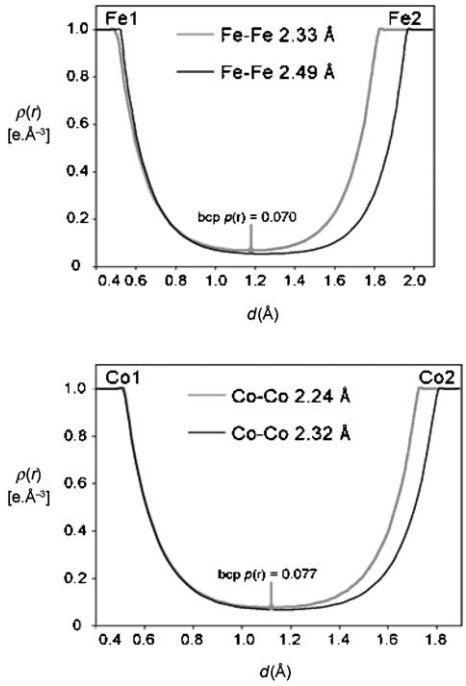

Figure 13. Electron density profiles $\rho(r)$ along the metal–metal vector for the mono-H complexes **1b** (Fe, top) and **12** (Co, bottom). The black lines refer to the fully optimized models, and the gray lines to those with a short arbitrarily fixed M–M distance. The latter cases are the only ones to exhibit a bcp. The $\rho(r)$ cutoff value is 1.0 e Å^{-3}.

refer to the fully optimized and constrained models. The common origin is fixed at the left metal atom and, in any case, the electron density starts to descend very steeply at about 0.55 Å with practically the same gradient. A flat plateau of almost equal electron density is invariably reached.

The longer the M–M separation, the wider is the plateau, and the longer the gradient remains invariant. For this reason, the detection of the bcp is possible only if the M–M distance is short enough to allow a sufficiently rapid and symmetric inversion of gradient. For the cobalt case (Figure 13, bottom), the curve of the stationary point and the model exhibiting the bcp are rather comparable. In contrast, the difference is more significant for the diiron system, where the Fe–Fe distance must be two times shorter before the bcp appears. In particular, the curve relative to the fully optimized geometry presents a quite extended zero-gradient region. As previously discussed, the presence of the phosphido bridge stretches the Fe–Fe separation to a point at which the H bridge has only limited influence over the M–M bond. This does not occur for the dicobalt complex, in which the overall Co–Co and the Co-H-Co bridge bonding are more directly correlated.

The appearance of the bcp at shorter M–M distances is attributable to the improved overlap between the metal atoms with a concentration of higher electron density in the intermetallic region. Recall that M–M bonding, which mainly results from the overlap of contracted d orbitals, may significantly differ from the typical M–L or intraligand bonds, in which the electrons of the contributing s and p orbitals are in diffuse lobes, properly aligned with the bonding direction.

The AIM method also allows quantification of interatomic interactions through the evaluation of the delocalization indices between basins δ_{A-B}.[42,43] In the mono-H diiron model **1b**, the δ(Fe–H) indexes are all slightly less than 0.5, while δ(Fe–Fe) has a higher value (about 0.62) which is almost as large as that of δ(Fe–PH_3). Importantly, in the bis-H derivative **4b**, the δ(Fe–Fe) of 0.30 is practically halved with respect to **1b**. As remarked by other authors,[14] the M–M delocalization indices follow the trends of the Mayer bond indices, which also predict Fe–Fe bond weakening in going from **1b** to **4b**. As another significant result, the AIM charge Q(Fe) in **1b** is significantly greater than in **4b**, which again supports the idea that the metal configuration changes from d^7 to d^6. This is also consistent with the determined Laplacian maps, which show a significant M–M depletion. The backdonation capabilities of the metals must decrease accordingly. A completely analogous picture applies to the dicobalt derivatives **12** and **13**, for which δ(Co–Co) decreases from 0.73 to 0.31.

In conclusion, the AIM delocalization indexes fully confirm that, in all the studied systems, there is significant M–M bonding, but the strength of interaction decreases when the bond is protonated. Thus, this approach reveals the unusual inconsistency between bond length and strength in the diiron system.

Conclusion

One axiom in chemistry is that the transformation of a 2e–2c bond into a 2e–3c one weakens the interaction between the two pivotal atoms. Also, the direct correlation between bond strength and bond length is a widely accepted paradigm.

Herein we have addressed a rare case in which these principles are apparently contradicted. Different theoretical strategies (quantitative and qualitative MO theory as well as the QTAIM method) were applied to understand the electronic underpinnings of Fe–Fe bond shortening on protonation of $[(CO)_2Fe(\mu\text{-dppm})(\mu\text{-P}t\text{Bu}_2)(\mu\text{-H})Fe(CO)_2]$. Gas-phase optimizations are consistent with the experimentally observed shortening of the Fe–Fe distance in the bis-H derivative **4** with respect to the mono-H precursor **1** and exclude the possibility of a solid-state origin of the effect. On the other hand, no M–M bond shortening was detected in comparable studies on the diiridium (**9**–**10**) and dicobalt (**12**–**13**) complexes. Noteworthily, these are also relevant for providing the first structural characterization of known and unknown protonation products of the $[\{CpM(CO)\}_2]$ compounds (M = Co, Ir). An active M–M bent bond is observed in all the mono-H bridged species, which is then oxidized on protonation with transfer of the bonding electron pair into the new hydrido bridge (oxidative addition). The bond strength indicators (e.g., the Mayer and AIM delocalization indexes) confirm the expected M–M bond weakening even when the distance is shortened rather than elongated. Accordingly, the direct correlation between bond length and strength is reversed. The failure of such a chemical paradigm has also been pointed out by Frenking et al.,[44] who calculated bond dissociation energies (BDE) of the M–P bond (M = Cr, Mo, W) for differently substituted phosphane ligands. In this present case, however, the origin of the phenomenon is not substituent-dependent but regulated by more subtle effects.

As is often observed for dimeric transition metal complexes, the AIM method has problems in detecting M–M bonding due to the absence of the expected bcp. Given a large degree of variance for the M–M distance, the present case study has highlighted how the gradient of electron density becomes suitable to define the bcp only below a certain lower limit of M–M distance.

In the case of the diiron system, the flat PES can also be associated with the presence of the phosphido bridge, which imposes a rather long M–M distance already in the mono-H system. Thus, it is not totally surprising that an already stretched bond cannot be definitely elongated on the transformation into a 2e–3c bond. The low energetic cost for rearranging the geometry of M-H-M systems like the present ones may have significant implications for organometallic, catalytic, and biological metal–hydrogen chemistry.

Finally, this paper has addressed current and crucial aspects of the combined usage of MO and electron density (QTAIM) analyses, which have recently been a source of controversy[45–47] and public debate.[48] Here we show how their complementary usage can provide more in-depth chemical information.

Computational Details

Becke's three-parameter hybrid exchange-correlation functional[49] and the nonlocal gradient correction of Lee, Yang, and Parr[50] (B3LYP) were used for DFT calculations with the Gaussian 98 program suite.[51] All of the fully optimized structures were confirmed as minima by calculation of the vibrational frequencies. All the reported wavenumbers were properly scaled.[52] The metal atoms were treated with the effective core potentials of Hay and Wadt[53] with the associated double-ζ valence basis functions. The basis set used for the remaining atomic species was 6-31G with the addition of the polarization functions (d, p) for all atoms, including hydrogen.[54] The reported protonation energies were simply calculated as the difference of the total energies between the protonated and the precursor models optimized in the gas phase. Qualitative MO arguments were derived from EHMO calculations[25] with the graphic capabilities of the package CACAO.[26] The AIM2000 package (vers. 1.0)[55] was used for the QTAIM bonding analysis.[11] To avoid the problems related to the core potentials of the metals, the corresponding wavefunctions were obtained from single-point calculations by using the basis set 6-311++G-(2d,2p) for the metals and bridging atoms. The M–M profiles were con-

structed with the PROFIL program as part of the AIMPAC suite of programs.[56]

Acknowledgements

Most of the computations were carried out at the CINECA of Bologna under the agreement CINECA-CNR. Thanks are given to Professors A. Sironi and P. Macchi (Università di Milano) and R. Bianchi (ISTM-CNR, Milano) for helpful discussions.

[1] a) *Recent Advances in Hydrides Chemistry* (Eds.: M. Peruzzini, R. Poli), Elsevier, Amsterdam, **2001**; b) G. J. Kubas, *Metal Dihydrogen and σ-Bond* Complexes, Kluwer Academic/Plenum Publishers, New York, **2001**; c) *Transition Metal Hydrides* (Ed.: A. Dedieu), VCH Publishers, New York, **1991**.
[2] A. Ienco, M. J. Calhorda, J. Reinhold, F. Reineri, C. Bianchini, M. Peruzzini, F. Vizza, C. Mealli, *J. Am. Chem. Soc.* **2004**, *126*, 11954.
[3] J. W. Peters, W. N. Lanzilotta, B. J. Lemon, L. C. Seefelft, *Science* **1998**, *282*, 1853.
[4] F. Gloaguen, J. D. Lawrence, T. B. Rauchfuss, M. Bénard, M.-M. Rohmer, *Inorg. Chem.* **2002**, *41*, 6573.
[5] M.-H. Baik, R. A. Friesner, G. Parkin, *Polyhedron* **2004**, *23*, 2879, and references therein.
[6] a) L. B. Handy, J. K. Ruff, L. F. Dahl, *J. Am. Chem. Soc.* **1970**, *92*, 7312; b) J. Roziere, J. M. Williams, R. P. , Stewart, Jr., J. L. Petersen, L. F. Dahl, *J. Am. Chem. Soc.* **1977**, *99*, 4497.
[7] a) D. J. Elliot, G. Ferguson, D. G. Holah, A. N. Hughes, M. C. Jennings, V. R. Magnuson, D. Potter, R. J. Puddephatt, *Organometallics* **1990**, *9*, 1336; b) D. J. Elliot, J. J. Vittal, R. J. Puddephatt, D. G. Holah, A. N. Hughes, *Inorg. Chem.* **1992**, *31*, 1247.
[8] Cambridge Structural Database System, version 5.22 (October **2001**), Cambridge Crystallographic Data Centre, 12 Union Road, Cambridge CB21EZ (UK).
[9] C. Bo, J.-M. Poblet, M. Costas, J.-P. Sarasa, *J. Mol. Struct.* **1996**, *371*, 37.
[10] More likely, the M–M bonding character should be searched in lower energy filled MOs if the hypothesis of σ bonding between pyramidal and T-shaped fragments is valid.
[11] R. F. W. Bader, *Atoms in Molecules, A Quantum Theory* **1994**, Clarendon Press, Oxford.
[12] a) C. Woodcock, R. Eisenberg, *Inorg. Chem.* **1985**, *24*, 1285; b) C. P. Kubiak, C. Woodcock, R. Eisenberg, *Inorg. Chem.* **1982**, *21*, 2119.
[13] C. Bo, M. Costas, J. M. Poblet, M.-M. Rohmer, M. Benard, *Inorg. Chem.* **1996**, *35*, 3298.
[14] P. Macchi, A. Sironi, *Coord. Chem. Rev.* **2003**, *238–239*, 383.
[15] H.-C. Böttcher, K. Merzweiler, C. Wagner, *Z. Anorg. Allg. Chem.* **1999**, *625*, 857.
[16] H.-C. Böttcher, C. Bruhn, K. Merzweiler, *Z. Anorg. Allg. Chem.* **1999**, *625*, 586.
[17] H.-C. Böttcher, H. Hartung, A. Krug, B. Walther, *Polyhedron* **1994**, *13*, 2893.
[18] H.-C. Böttcher, M. Graf, K. Merzweiler, C. Wagner, *J. Organomet. Chem.* **2001**, *628*, 144.
[19] R. Hoffmann, *Angew. Chem.* **1982**, *94*, 711; *Angew. Chem. Int. Ed. Engl.* **1982**, *21*, 711.
[20] D. M. Heinekey, D. A. Fine, D. Barnhart, *Organometallics* **1997**, *16*, 2530.
[21] a) S. Stella, C. Floriani, A. Chiesi-Villa, C. Guastini, *New J. Chem.* **1988**, *12*, 621; b) M. Enders, G. Ludwig, H. Pritzkow, *Organometallics* **2001**, *20*, 827; c) P. Louca, J. A. K. Howard, *Acta Crystallogr. Sect. C* **1987**, *43*, 1908; d) F. Baumann, E. Dormann, Y. Ehleiter, W. Kaim, J. Kärcher, M. Kelemen, R. Krammer, D. Saurenz, D. Stalke, C. Wachter, G. Wolmershäuser, H. Sitzmann, *J. Organomet. Chem.* **1999**, *587*, 267; e) W. I. Bailey, Jr., D. M. Collins, F. A. Cotton, J. C. Baldwin, W. C. Kaska, *J. Organomet. Chem.* **1979**, *165*, 373; f) F. E. Ginsburg, L. M. Cirjak, L. F. Dahl, *J. Chem. Soc. Chem. Commun.* **1979**, 468; g) L. M. Cirjak, F. E. Ginsburg, L. F. Dahl, *Inorg. Chem.* **1982**, *21*, 940.
[22] P. Macchi, A. Sironi, *J. Am. Chem. Soc.* **2005**, *127*, 16494.
[23] R. F. W. Bader, C. F. Matta, F. Cortés-Guzmán, *Organometallics* **2004**, *23*, 6253.
[24] I. Mayer, *Chem. Phys. Lett.* **1983**, *97*, 270.
[25] a) R. Hoffmann, W. N. Lipscomb, *J. Chem. Phys.* **1962**, *36*, 2872; b) R. Hoffmann, W. N. Lipscomb, *J. Chem. Phys.* **1962**, *37*, 3489.
[26] a) C. Mealli, D. M. Proserpio, *J. Chem. Educ.* **1990**, *67*, 399; b) C. Mealli, A. Ienco, D. M. Proserpio, *Book of Abstracts of the XXXIII ICCC*, Florence, **1998**, p. 510.
[27] E. Hunstock, C. Mealli, M. J. Calhorda, J. Reinhold, *Inorg. Chem.* **1999**, *38*, 5053.
[28] T. A. Barckholtz, B. E. Bursten, *J. Organomet. Chem.* **2000**, *596*, 212.
[29] H. Jacobsen, T. Ziegler, *J. Am. Chem. Soc.* **1996**, *118*, 4631.
[30] Y. Xie, H. F. Schaefer III, R. B. King, *J. Am. Chem. Soc.* **2000**, *122*, 8746.
[31] No significant difference is observed for the M–Cp bond strength on going from the mono-H and bis-H derivatives of both iridium and cobalt species.
[32] For both the Ir and Co systems, the CO-bridged precursors have the lowest wavenumbers for symmetric and asymmetric vibrations (1672–1718 and 1789–1835 cm^{-1} for the iridium and cobalt species **8** and **11**, respectively). The values for the iridium series with terminal CO ligands are 1848–1871, 1931–1946, and 2006–2014 cm^{-1} in models **8b**, **9**, and **10**, respectively. For the protonated dicobalt complexes **12** and **13**, the pairs of values 2034–2050 and 2133–2136 cm^{-1} are indicative of a less efficient backdonation with respect to the iridium analogues, obviously on account of the reduced diffuseness of the metal d orbital, and hence a smaller metal–ligand overlap. In all cases, the geometric and spectroscopic data confirm progressive change of the formal metal configuration from d^8 to d^6.
[33] B. E. Hanson, P. E. Fanwick, J. S. Mancini, *Inorg. Chem.* **1982**, *21*, 3811.
[34] G. Hogarth, M. H. Lavender, K. Shukri, *Organometallics* **1995**, *14*, 2325.
[35] a) H.- C. Böttcher, M. Graf, K. Merzweiler, C. Wagner, *Inorg. Chim. Acta* **2003**, *350*, 399; b) A. A. Low, K. L. Kunze, P. J. MacDougall, M. N. Hall, *Inorg. Chem.* **1991**, *30*, 1079.
[36] A. Phillips and C. Mealli, unpublished results.
[37] C. Bo, J.-P. Sarasa, J.-M. Poblet, *J. Phys. Chem.* **1993**, *97*, 6362.
[38] C. Mealli, D. M. Proserpio, *J. Organomet. Chem.* **1990**, *386*, 203.
[39] J. Reinhold, E. Hunstock, C. Mealli, *New J. Chem.* **1994**, *18*, 465.
[40] R. Bianchi, G. Gervasio, D. Marabello, *Inorg. Chem.* **2000**, *39*, 2360.
[41] R. Bianchi, G. Gervasio, D. Marabello, *Acta Crystallogr. Sect. B* **2001**, *57*, 638.
[42] R. F. W. Bader, M. E. Stephens, *J. Am. Chem. Soc.* **1975**, *97*, 7341.
[43] The index $\delta_{A-B} = F(A,B) + F(B,A)$ measures the extent of electron exchange or sharing between two adjacent atomic basins A and B. $F(A,B) = F(B,A)$ represents the combined summation of the S_{ij} elements of the atomic overlap matrix $-\Sigma_i \Sigma_j S_{ij}(A) S_{ij}(B)$.
[44] G. Frenking, K. Wichmann, N. Fröhlich, J. Grobe, W. Golla, D. Le Van, B. Krebs, M. Läge, *Organometallics* **2002**, *21*, 2921.
[45] R. J. Gillespie, P. L. A. Popelier, *From Lewis to Electron Densities*, Oxford University Press, New York **2001**.
[46] G. Frenking, *Angew. Chem.* **2003**, *115*, 152; *Angew. Chem. Int. Ed.* **2003**, *42*, 143.
[47] R. F. W. Bader, *Int. J. Quantum Chem.* **2003**, *94*, 173.
[48] Proceedings from the Euresco Conference on New Theoretical and Spectroscopic Approaches to Inorganic Chemistry Problems (chairpersons: C. Mealli, S. Alvarez), Sant Feliu du Guixol (Spain), **2004** (http://www.esf.org/euresco/04/pc04018).
[49] A. D. Becke, *J. Chem. Phys.* **1993**, *98*, 5648.
[50] C. Lee, W. Yang, R. Parr, *Phys. Rev. B* **1988**, *37*, 785.
[51] Gaussian 98, Revision A.7, M. J. Frisch, G. W. Trucks, H. B. Schlegel, G. E. M. Scuseria, A. Robb, J. R. Cheeseman, V. G. Zakrzewski, J. A. Montgomery, R. E. Stratmann, J. C. Burant, S. Dapprich, J. M. Millam, A. D. Daniels, K. N. Kudin, M. C. Strain, O. Farkas, J. Tomasi, V. Barone, M. Cossi, R. Cammi, B. Mennucci, C. Pomelli,

C. Adamo, S. Clifford, J. Ochterski, G. A. Petersson, P. Y. Ayala, Q. Cui, K. Morokuma, D. K. Malick, A. D. Rabuck, K. Raghavachari, J. B. Foresman, J. Cioslowski, J. V. Ortiz, B. B. Stefanov, G. Liu, A. Liashenko, P. Piskorz, I. Komaromi, R. Gomperts, R. L. Martin, D. J. Fox, T. Keith, M. A. Al-Laham, C. Y. Peng, A. Nanayakkara, C. Gonzalez, M. Challacombe, P. M. W. Gill, B. G. Johnson, W. Chen, M. W. Wong, J. L. Andres, M. Head-Gordon, E. S. Replogle, J. A. Pople, Gaussian, Inc., Pittsburgh, PA, **1998**.
[52] A. P. Scott, L. Random, *J. Chem. Phys.* **1996**, *100*, 16502.
[53] P. J. Hay, W. R. Wadt, *J. Chem. Phys.* **1985**, *82*, 299.
[54] P. C. Hariharan, J. A. Pople, *Theor. Chim. Acta* **1973**, *28*, 213.
[55] AIM2000: A Program to Analyze and Visualize Atoms in Molecules: F. Biegler-König, J. Schönbohm, B. Bayles, *J. Comput. Chem.* **2001**, *22*, 545.
[56] F. Biegler-König, R. F. W. Bader, T.-H. Tang, *J. Comput. Chem.* **1982**, *3*, 317.

Received: August 31, 2005
Revised: December 16, 2005
Published online: April 6, 2006

